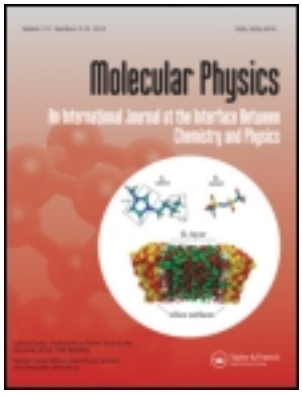

Molecular Physics: An International Journal at the Interface Between Chemistry and Physics
Publication details, including instructions for authors and subscription information:
http://www.tandfonline.com/loi/tmph20

Vibronic valence and Rydberg transitions in geminal chloro-fluoro-ethene (1,1-C_2H_2FCl): a spectroscopic and quantum chemical investigation

R. Locht[a], D. Dehareng[b] & B. Leyh[a]
[a] Department of Chemistry, Molecular Dynamics Laboratory, University of Liège, Liège, Belgium
[b] Department of Live Sciences, Centre for Protein Engineering, University of Liège, Liège, Belgium

Accepted author version posted online: 10 Sep 2013.Published online: 07 Oct 2013.

To cite this article: R. Locht, D. Dehareng & B. Leyh (2014) Vibronic valence and Rydberg transitions in geminal chloro-fluoro-ethene (1,1-C_2H_2FCl): a spectroscopic and quantum chemical investigation, Molecular Physics: An International Journal at the Interface Between Chemistry and Physics, 112:11, 1520-1539, DOI: 10.1080/00268976.2013.842659

To link to this article: http://dx.doi.org/10.1080/00268976.2013.842659

Molecular Physics, 2014
Vol. 112, No. 11, 1520–1539, http://dx.doi.org/10.1080/00268976.2013.842659

RESEARCH ARTICLE

Vibronic valence and Rydberg transitions in geminal chloro-fluoro-ethene (1,1-C_2H_2FCl): a spectroscopic and quantum chemical investigation

R. Locht[a,*], D. Dehareng[b] and B. Leyh[a]

[a]*Department of Chemistry, Molecular Dynamics Laboratory, University of Liège, Liège, Belgium;* [b]*Department of Live Sciences, Centre for Protein Engineering, University of Liège, Liège, Belgium*

(*Received 17 June 2013; accepted 4 September 2013*)

The vacuum ultraviolet photoabsorption spectrum of 1,1-C_2H_2FCl has been examined in detail between 5 and 15 eV photon energy by using synchrotron radiation dispersed by three different monochromators. Quantum chemical calculations are performed to help in the analysis of the valence/Rydberg transition region centred at 7.05 eV including the $3a''(\pi)\rightarrow\pi^*$ and the $3a''(\pi)\rightarrow 3s$ Rydberg transitions. Interactions between states involving transitions to the 3s, 4d and σ^* orbitals are identified. A vibrational analysis is proposed for the structures belonging to these transitions. For the $\pi(3a'')\rightarrow\pi^*$ transition, one vibrational progression is observed with $\omega_3 = 1410 \pm 50$ cm^{-1} and its lowest excitation energy is determined at about 6.398 ± 0.003 eV. The $\pi(3a'')\rightarrow 3s$ Rydberg transition is characterised by a single progression with $\omega_3 = 1410 \pm 80$ cm^{-1} likely starting at about 6.45 eV. These vibrations are ascribed to the C=C stretching motion. The abundant structure observed in the spectrum between 7.8 and 10.5 eV has been analysed in terms of vibronic transitions to *n*s ($\delta = 0.97$), *n*p ($\delta = 0.63$ and 0.40) and *n*d ($\delta = 0.13$ and -0.11) Rydberg states, which belong to series converging to the 1,1-$C_2H_2FCl^+(\tilde{X}^2A'')$ ionic ground state. The analysis of the vibrational structure of the individual Rydberg states has been attempted leading to average values of the wave numbers $\omega_3 = 1420 \pm 20$ cm^{-1}, $\omega_7 = 720 \pm 50$ cm^{-1} and $\omega_9 = 390 \pm 50$ cm^{-1}. Between 10.5 and 12.5 eV, nine other Rydberg states converging to the 1,1-$C_2H_2FCl^+(\tilde{A}^2A')$ first excited state were analysed by the same way. The vibrational structure of these Rydberg states results from the excitation of one vibrational normal mode ν_7 with an average value of $\omega_7 = 520 \pm 20$ cm^{-1}, which is assigned to the C–Cl stretching vibration as inferred from quantum chemical calculations.

Keywords: vacuum UV photoabsorption; synchrotron radiation; quantum chemical calculations; valence and Rydberg transitions; 1,1-C_2H_2FCl

1. Introduction

The influence of the position and nature of the substituent(s) on the dynamics of the molecular ions has been investigated on ethylene and a few of its halogenated derivatives, e.g. on C_2H_3F [1], C_2H_3Cl [2] and C_2H_3Br [3], but also on C_2H_2FCl (1,1- and 1,2-isomers) [4], and more recently on 1,1-$C_2H_2F_2$ [5] using vacuum ultraviolet (VUV) photoabsorption and photoelectron spectroscopies. The ionisation and dissociation dynamics were investigated by photoionisation mass spectrometry and photoelectron–photoion coincidence spectroscopy. *Ab initio* quantum chemical calculations were applied to support the different aspects of the interpretation of the numerous experimental results.

To our knowledge the earliest VUV photoabsorption work on the 1,1-C_2H_2FCl molecule has been reported by Scott and Russell [6] together with two other fluorochloro-substituted ethylenes. This study was restricted to the 1200–2200 Å (5.635–10.332 eV) spectral range. A classification of the Rydberg transitions and their vibrational analysis has been proposed.

Tornow *et al*. [4] have investigated the three isomers of C_2H_2FCl between 6.0 and 13.0 eV by low-resolution VUV photoabsorption spectroscopy using synchrotron radiation as a light source. The observed transitions have been assigned to valence–valence and valence–Rydberg transitions. For a few Rydberg states, the vibrational structure could be observed and has been analysed. In addition, the HeI (21.22 eV) and NeI (16.67–16.85 eV) photoelectron spectra of these compounds have been measured. The successive ionisation energies have been interpreted with the help of MNDO calculations. Assignments of the observed vibrational structure have been reported.

The VUV photoabsorption spectroscopic data reported in the literature on 1,1-C_2H_2FCl remain very scarce. The present paper reports on the VUV photoabsorption spectrum (PAS) of the 1,1-C_2H_2FCl molecular system obtained at higher resolution in the 5.0–15.0 eV spectral region. Interpretation and assignments of several additional spectral features are supported by *ab initio* quantum chemical calculations.

*Corresponding author. Email: robert.locht@ulg.ac.be

2. Experimental

2.1. Experimental set-up

The experimental set-ups used in this work have already been described in detail previously [1,3]. Only the most salient features will be reported here. Furthermore, three monochromators were available in the laboratory and at the BESSY synchrotron radiation facilities.

Synchrotron radiation available from the BESSY I facility (Berlin, Germany) was dispersed with a modified VUV normal incidence 225 McPherson monochromator with a focal length of 1.5 m, instead of 1 m in the commercial version (1m-NIM-2 beam line). A laminar Zeiss grating is used for the efficient reduction of the second spectral order. It is gold coated with 1200 lines mm^{-1} and its transmission breaks down above 26 eV (210,000 cm^{-1} or 48 nm). The width of the entrance and exit slits of 100 μm ensures a 0.1-nm wavelength resolution corresponding to a resolving power of about 1200 at 10 eV (124 nm). This monochromator has been used for recording the low-resolution absolute photoabsorption spectra in the 5–13 eV photon energy range [4].

In the laboratory, a commercial version of the 1m-NIM 225 McPherson monochromator is equipped with an Al grating of 1200 lines mm^{-1}. The light source is a commercial Ophthos Kr-microwave discharge lamp allowing us to scan between 125 nm (9.92 eV) and 165 nm (7.51 eV). The slit widths were adjusted at 25–50 μm providing a 0.02-nm wavelength resolution corresponding to a resolving power of about 5000 at 10 eV.

The 3m-NIM monochromator at the 3m-NIM2 beam line at BESSY II (Berlin, Germany) is positioned at a bending magnet front end. It is equipped with two spherical gratings, i.e. an Al/MgF_2 grating of 600 lines mm^{-1} and a Pt grating of 2400 lines mm^{-1}. The entrance and exit slits were adjusted between 10 and 40 μm leading to a resolving power of about 25,000–13,000 at 10 eV photon energy. This monochromator was used for recording high-resolution spectra. Most of the spectra discussed in the present work were measured with 40-μm entrance and 10-μm exit slits, using the 600-lines mm^{-1} Al/MgF_2 grating.

In all the set-ups described above, the light has to travel through a 1-mm thick stainless steel microchannel plate located at the exit slit of the monochromator, in order to maintain a differential pressure rate of 1:1000, before entering a 30-cm long stainless steel absorption cell. The vapour pressure in the cell is measured by a Balzers capacitor manometer. The light is detected by a sodium salicylate sensitised photomultiplier located at the end of the absorption cell and in front of the absorption cell entrance slit. Output pulses are recorded by a 100-MHz counter. The recording of an absorption spectrum requires one scan with gas in the absorption cell and one with the evacuated cell. The stability of the synchrotron radiation and of the pressure in the cell ensured reliable absorption data. If necessary, the spectra presented in the following sections were corrected for any pressure drift.

Two different samples of 1,1-C_2H_2FCl have been used. A first sample was prepared in the laboratory as described earlier [4] with a 99.9% gas chromatographic purity and a boiling point of $-24\ ^{\circ}C$. The commercially available 1,1-C_2H_2FCl, purchased from ABCR GmbH and of 98% purity, was used without further purification.

2.2. Data handling and error estimation

As will be mentioned in the next sections, weak sharp peaks and diffuse structures are often superimposed on a strong continuum. To make the characterisation of these features easier, a continuum subtraction procedure has been applied. The mathematical background of this digital data processing method has been set out in detail by Carbonneau *et al.* [7], Marchand [8] and Marmet [9]. The parameters of this filter have been evaluated by Morawski [10]. This digital filtering by 'straightening through smoothing' [8] was first applied to a large number of atomic and molecular spectra excited by electron impact [11–13]. Later, its application has been extended to e.g. photoionisation mass spectrometry [14], photoelectron [15] and photoabsorption [5] spectroscopy. Briefly, for this purpose, the experimental curve is strongly smoothed to simulate the underlying continuum which is then subtracted from the original spectrum. The smoothing procedure consists of filtering the experimental curve by fast Fourier transform (FFT). The weak features then emerge from a remaining strongly attenuated background. The resulting diagram will be called Δ plot in the forthcoming sections. To verify that no weak structure has been removed by this operation, the same procedure is applied to the subtracted continuum. The resulting residue is a signal oscillating around zero with about two orders of magnitude lower amplitude.

The wavelength calibration of the 1.5m-NIM and 3m-NIM monochromators has been performed by using the Ar absorption spectrum between the $^2P_{3/2}$ and the $^2P_{1/2}$ ionic states. The accuracy of this calibration is better than 2 meV. In the measurements between 5 and 15 eV photon energy, the PAS has been recorded with energy steps of about 10 meV. The uncertainty on the energy position of a feature is estimated to be 6 meV. In the photoabsorption spectra recorded between 6 and 10 eV and between 9 and 15 eV, an energy increment of 1 meV has been adopted. The uncertainty on the energy position of a feature is estimated to be of the order of 3 meV. This evaluation is confirmed by the reproducibility of energy positions measured in different spectra recorded over several years.

3. Experimental results

The VUV PAS of 1,1-C_2H_2FCl as measured between 5 and 15 eV photon energy (with 10-meV increments) with the

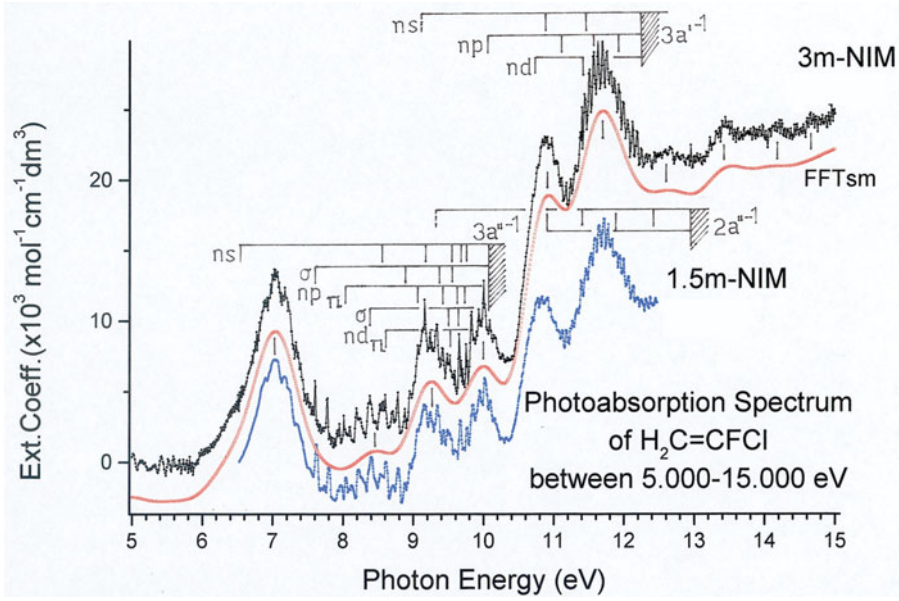

Figure 1. VUV photoabsorption spectrum (in terms of the molecular extinction coefficient $\varepsilon_{h\nu}$) of 1,1-C_2H_2FCl between 5 and 15 eV photon energy obtained with the 3m-NIM monochromator. The same spectrum (blue line, slightly shifted down the *y*-scale) measured with the 1.5m-NIM [4] is shown for comparison. Vertical bars and shaded areas locate Rydberg states and their convergence limits. The open dotted (red) curve represents the FFT strongly smoothed spectrum. Vertical lines locate valence–valence transitions.

3m-NIM monochromator is shown in Figure 1. The good control of the experimental parameters allows us to display the spectrum in terms of the molecular extinction coefficient $\varepsilon_{h\nu}$ as a function of the photon energy (eV). For comparison, the VUV PAS of the same compound as obtained earlier [4], but at lower resolution and slightly shifted on the $\varepsilon_{h\nu}$ scale, is shown in the same figure. The gain in resolution is obvious but the extinction coefficient is significantly larger for the high energy part of the spectrum. A continuous dotted (red) line drawn through the spectrum shows the underlying continuum obtained by FFT smoothing. Vertical lines indicate the valence (*V*) and Rydberg (*R*) transition energies. Their energy positions are listed in Table 1 and compared with previous results [4,6].

In contrast with our observations in the 1,1-$C_2H_2F_2$ VUV-PAS [5], Figure 1 clearly shows a regular fine structure spread over the whole photon energy range investigated in this work.

4. *Ab initio* calculations: methods and results

4.1. Computational tools

All the calculations were performed with the Gaussian 09 programme [17]. The basis set used for all the calculations is aug-cc-pVDZ [18], containing polarisation as well as diffuse functions. Some calculations were also performed without diffuse functions (basic cc-pVDZ).

The geometry optimisation of the neutral ground state has been performed at the CCSD(FC) [19,20], M06-2X(DFT) [21], PBE0(DFT) [22] and SAC-CI [23] levels in order to determine the vertical excitation energies for the low-lying excited states within different frameworks and cross-check them. The PBE0 functional was already recognised as well suited for describing low-lying Rydberg and valence excited states [24], and the M06-2X functional is a new functional generally considered as providing very satisfactory agreement on thermodynamical properties. A geometry optimisation of the first three excited states was performed at the UM06-2X and TDDFT [25] levels. The ground-state vibrational wave numbers were determined at the M06-2X level.

The geometry optimisation of the cationic $\tilde{X}^2A''$ ground state and of the first two excited $\tilde{A}^2A'$ and $\tilde{B}^2A''$ states was performed at the M06-2X ($\tilde{X}$ and $\tilde{A}$ states) and TDDFT ($\tilde{B}$ state) level. The molecular orbital configuration of 1,1-C_2H_2FCl in the C_S symmetry group is described by

$$1s(Cl)^2,\ 2s(Cl)^2,\ 1s(F)^2,\ 1s(C1)^2,\ 1s(C2)^2,\ 2p_{x,y,z}(Cl)^6$$
$$(1a')^2(2a')^2(3a')^2(4a')^2(5a')^2(1a'')^2(6a')^2(7a')^2(8a')^2(2a'')^2$$
$$(9a')^2(3a'')^2:\ \tilde{X}^1A',$$

where the 1a′ and 2a′ are the first outer valence shell orbitals. The 3a″ MO has a π character.

Table 1. Energy positions (eV), wave numbers (cm^{-1}) (in brackets) and assignments proposed for valence and Rydberg transitions in the vacuum UV PAS of 1,1-C_2H_2FCl between 5.0 and 15 eV. Comparison is made with the results and assignments of [4, 6]. Conversion factor 1 eV = 8065.545 cm^{-1} [16].

Valence transitions		
[6]	[4]	This work
7.012 (56,556)	7.14 (57,588)	7.01 (56,539)
	8.50 (68,557)	8.45 (68,154)
	9.20 (74,203)	9.27 (74,768)
	10.0 (80,655)	10.01 (80,736)
	10.85 (87,511)	10.93 (88,156)
	11.70 (94,367)	11.71 (94,448)
	–	12.65 (102,029)
	–	13.44 (108,401)
	–	~14.2 (114,531)
	–	14.6 (117,757)
Rydberg transitions		
Adiabatic convergence limit: 10.024 eV – $\tilde{X}^2A''$ [4]		
	3a″→*n*s	
6.509 (52,500)	–	6.645 (53,596)
8.406 (67,800)	8.60 (69,364)	8.535 (68,847)
9.108 (73,437)	9.21 (74,284)	9.186 (74,090)
9.420 (75,927)	9.49 (76,542)	9.482 (76,477)
9.584 (77,321)	9.65 (77,833)	9.654 (77,865)
9.688 (78,141)	9.75 (78,639)	9.758 (78,704)
	3a″→*n*pσ	
	7.61 (61,379)	7.608 (61,363)
	8.88 (71,622)	8.839 (71,291)
	9.33 (75,252)	9.316 (75,139)
	9.57 (77,187)	9.551 (77,034)
	9.66 (77,913)	–
	9.77 (78,800)	–
	3a″→*n*pπ	
	8.02 (64,686)	8.012 (64,621)
	8.92 (71,945)	9.065 (73,114)
	9.37 (75,574)	9.408 (75,880)
	9.57 (77,187)	9.597 (77,405)
	9.70 (78,236)	9.705 (78,276)
	9.77 (78,800)	9.841 (79,373)
		–
		–
		–
		9.920 (80,010)
	3a″→*n*d(σ)	
	8.38 (65,589)	8.387 (67,646)
	9.15 (73,800)	9.151 (73,808)
	9.44 (76,139)	–
	9.65 (77,832)	9.654 (77,865)
	9.75 (78,639)	9.758 (78,704)
	9.77 (78,800)	–
	3a″→*n*d(π)	
		8.601
		9.211
		9.501
		9.654
Adiabatic convergence limit: 12.236 eV – $\tilde{A}^2A'$ [4]		
	9a′→*n*s	
	9.17 (73,916)	–
	10.85 (87,511)	10.838 (87,414)
	11.38 (91,786)	11.448 (92,334)
	11.72 (94,528)	–
	11.88 (95,819)	–
	11.97 (96,556)	

(*continued*)

Table 1. (*Continued*).

Valence transitions		
[6]	[4]	This work
	9a′→*n*p	
		10.052 (81,075)
		11.115 (89,649)
		11.566 (93,286)
		11.802 (95,190)
		11.923 (96,165)
	9a′→*n*d	
		10.626 (85,704)
		11.377 (91,762)
Vertical convergence limit: 13.22 eV – $\tilde{B}^2A''$ [4]		
	2a″→*n*s	
		[9.25] (74,606)
		[11.4] (91,950)
	2a″→*n*p	
		[10.84] (87,430)
		[11.9] (95,980)

4.2. *Results of the calculations*

The results of the geometry optimisation are presented in Table 2, according to the numbering shown in the same table.

In the literature, the calculation level which is considered as the most accurate is CCSD(FC). However, the M06-2X is also recognised as a very good functional.

The wave numbers calculated for the vibrational normal modes represented in Figure 2 for the neutral ground state are listed in Table 3. In Table 4, the wave numbers related to the cationic ground and first two excited states are displayed. For the two excited states of the cation, a few vibrational modes are differing from the ground state of the ion. The ordering of the vibrational normal modes presented in this work follows the rules of nomenclature as proposed by Mulliken and Herzberg [26,27]. Experimental infrared [28,29] and Raman [30] spectroscopic results related to the neutral ground state are listed in Table 3 for comparison.

The vertical excitation energies to several valence states are presented in Table 5 at three calculation levels, all within the aug-cc-pVDZ basis set. For the first five excited states, all the calculation levels agree about the ordering of the states. It is therefore very likely that the three states around 7 eV are superimposed. From the two DFT calculations, the first two states are strongly mixed, preventing to obtain an optimised geometry for the second excited state at the PBE0 level. Since this level provides good descriptions of low-lying Rydberg and valence states [25], these results can be considered as confirming the results of the M06-2X level [24] as well. It has to be pointed out that the excited valence σ^* MO, which is antibonding on the C–Cl bond, is strongly mixed with a Rydberg 4d MO. Such

Table 2. Optimised geometry of the neutral and the ionic ground states and the first two cationic excited state in the C_S symmetry group at different calculation levels. Internuclear distances in Å and angles in degrees.

Neutral ground state – $\tilde{X}^1A'$					
Level	C1–C2	C2–H3	C2–H4	C1–F5	C1–Cl6
CCSD(FC)	1.3374	1.0917	1.0894	1.3498	1.7324
M06-2X	1.3231	1.0865	1.084	1.333	1.7251
	H3–C2–C1	H4–C2–C1	F5–C1–C2	Cl6–C1–C2	
CCSD(FC)	119.398	120.192	122.255	126.035	
M06-2X	119.163	120.133	122.876	125.739	
Cation ground state – $\tilde{X}^2A''$					
Level	C1–C2	C2–H3	C2–H4	C1–F5	C1–Cl6
CCSD(FC)	1.4214	1.0956	1.0938	1.293	1.6558
M06-2X	1.4098	1.0912	1.0893	1.2816	1.6497
	H3–C2–C1	H4–C2–C1	F5–C1–C2	Cl6–C1–C2	
CCSD(FC)	118.776	119.619	118.636	124.15	
M06-2X	118.726	119.667	119.085	123.962	
Cation first excited state – $\tilde{A}^2A'$					
Level	C1–C2	C2–H3	C2–H4	C1–F5	C1–Cl6
CCSD(FC)	1.3211	1.0965	1.0926	1.308	1.8741
M06-2X	1.3056	1.0942	1.0896	1.2891	1.879
	H3–C2–C1	H4–C2–C1	F5–C1–C2	Cl6–C1–C2	
CCSD(FC)	117.496	122.278	135.404	120.092	
M06-2X	117.366	122.706	136.75	118.469	
Cation second excited state – $\tilde{B}^2A''$					
Level	C1–C2	C2–H3	C2–H4	C1–F5	C1–Cl6
TD-DFT	1.3244	1.0959	1.0891	1.2617	2.0725
	H3–C2–Cl	H4–C2–C1	F5–C1–C2	Cl6–C1–C2	
TD-DFT	116.99	121.78	135.46	120.36	

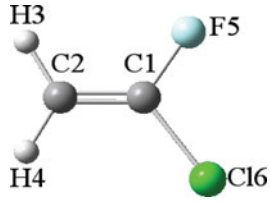

Rydberg–valence interactions involving σ^* antibonding orbitals and the associated 'rydbergisation' phenomenon have been recently reviewed [31].

To check this ordering of the excited states and the valence character of the [σ^* + 4d] state, the first vertical excitation energies were also determined at the TDDFT/M06-2X level using a basis set without diffuse functions, i.e. cc-pVDZ basis set (see Table 5). These results suggest that a valence $\pi \rightarrow \sigma^*$ and a Rydberg $\pi \rightarrow$ 3s transitions should be below or close to the $\pi \rightarrow \pi^*$ transition.

The optimised geometries of the first three excited states are displayed in Table 6 together with the corresponding adiabatic excitation energies.

The optimised geometry of the first excited state is characterised by a very large C–Cl bond length, very likely related to the antibonding character of the MO populated by the excitation. The 3s-like Rydberg orbital does not show this feature, but the [σ^* + 4d] MO involved in the excitation of the first two states does. The first excited state, showing a mixed character at the vertical excitation energy, is adiabatically correlated with the [σ^* + 4d] state. This state exhibiting a dissociative character, its excitation would produce a broad continuous band. The second state, correlating with the 3s Rydberg state, has to be observed, but owing to its closeness with the π^* state, the experimental determination of the adiabatic ionisation energies is expected to be difficult. A schematic representation of the situation described by the present calculations is displayed in Figure 3.

5. Analysis of the experimental data and discussion

We also measured the HeI-PES [4] and the threshold photoelectron spectrum (TPES) of 1,1-C_2H_2FCl, which will be reported in a forthcoming publication [32]. The first adiabatic ionisation energy IE_{ad}(1,1-$C_2H_2FCl^+$,$\tilde{X}^2A''$) is equal to 10.024 ± 0.003 eV [4] or 10.018 ± 0.007 eV [32]. The corresponding vertical value

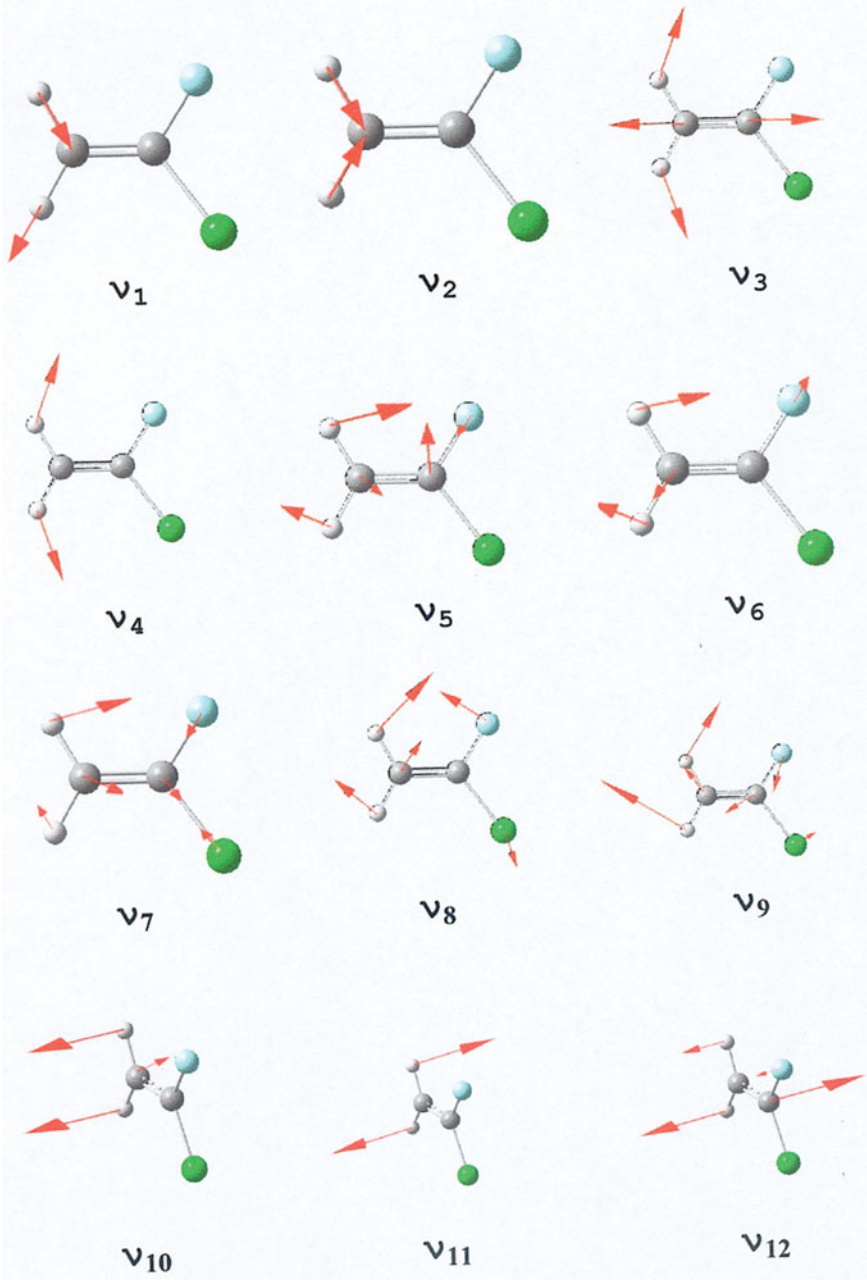

Figure 2. Graphical representation of the 12 vibrational normal modes of 1,1-C_2H_2FCl in the C_S symmetry point group for which the associated wave numbers have been calculated.

$IE_{vert}(1,1\text{-}C_2H_2FCl^+, \tilde{X}^2A'')$ is equal to 10.201 ± 0.003 eV [4] or 10.198 ± 0.007 eV [32]. The first excited state of the cation exhibits an extended vibrational structure starting at $IE_{ad}(1,1\text{-}C_2H_2FCl^+, \tilde{A}^2A') = 12.236 \pm 0.003$ eV [4] or 12.238 ± 0.007 eV [32]. The corresponding vertical values are $IE_{vert}(1,1\text{-}C_2H_2FCl^+, \tilde{A}^2A') = 12.368 \pm 0.003$ eV [4] and 12.428 ± 0.007 eV [32]. This latter discrepancy corresponds to one vibrational quantum.

At higher energies, five bands are observed by HeI-PES [4] and are characterised by their vertical ionisation energies at 13.22, 14.25, 14.93, 17.17 and 17.69 eV. In the TPES measured between 9.9 and 25 eV, one additional maximum is observed at 20.208 eV [32].

In the absence of any prior information on the extent of possible Rydberg–Rydberg interactions, a first zero-order assignment of the spectral lines will be attempted, fitting the simple Rydberg formula (1) for the positions in energy

Table 3. Vibrational wave numbers of the neutral ground state as calculated at the BLYP, B3LYP and M06-2X levels using the aug-cc-pVDZ basis set. The recommended scaling factors are given in parentheses. Comparison is made with experimental values obtained by IR [28, 29] and Raman [30] spectroscopy.

	Wave numbers (cm^{-1})					
	Experiment			Theory		
	[28]	[29]	[30]	BLYP (0.99)[a]	B3LYP (0.96)[a]	M06-2X (0.96)[b]
a′						
ν_1	3055	3071	3069	3217 (3185)	3297 (3165)	3328 (3195)
ν_2	3015	3018	3016	3109 (3078)	3187 (3060)	3210 (3082)
ν_3	1645	1654	1656	1641 (1625)	1713 (1644)	1754 (1684)
ν_4	1383	1380	1383	1352 (1338)	1389 (1333)	1391 (1335)
ν_5	1189	∼1184	1186	1110 (1099)	1167 (1120)	1209 (1161)
ν_6	937/953	946	947	898 (889)	940 (902)	963 (924)
ν_7	693/707	698/709	699	652 (645)	687 (660)	704 (676)
ν_8	–	432	432	409 (405)	426 (409)	433 (416)
ν_9	–	370	371	357 (353)	369 (354)	370 (355)
a″						
ν_{10}	835	834	836	829 (821)	875 (840)	901 (865)
ν_{11}	621	–	607	683 (676)	713 (684)	727 (698)
ν_{12}	516	519	515	499 (494)	523 (502)	530 (509)

[a]See [35].
[b]See [21].

E_{Ryd} of the successive features:

$$E_{Ryd} = IE - \frac{R}{(n-\delta)^2} = IE - \frac{R}{(n^*)^2}, \qquad (1)$$

where R is the Rydberg constant ($R = 13.6057$ eV) [16], δ is the quantum defect, n^* is the effective quantum number and IE is the convergence limit of the considered Rydberg series. The successive ionisation energies IE to be used in this work have been defined earlier in this section and are inserted in Figure 1. The fine structure observed in the spectrum will be assigned mainly to vibrational excitation associated with the successive Rydberg series rather than to Rydberg states with high principal quantum number n. In the former case, the intensity distribution follows the Franck–Condon distribution whereas in the latter the intensity follows the n^{-3} law. Robin [34] made an extensive and critical review of the analyses of Rydberg transitions and proposed rules and guidelines for assignments.

Table 4. Wave numbers (cm^{-1}) related to the vibrational normal modes of 1,1-C_2H_2FCl in its ground state and of 1,1- $C_2H_2FCl^+$ in its ground $\tilde{X}^2A''$ and first two excited $\tilde{A}^2A'$ and $\tilde{B}^2A''$ states as calculated at the M06-2X level ($\tilde{X}$ and $\tilde{A}$ states) and TDDFT ($\tilde{B}$ state). In parentheses are given the values corrected for the chosen scale factor of 0.96 [21].

State	$\tilde{X}^1A'$	$\tilde{X}^2A''$	$\tilde{A}^2A'$	$\tilde{B}^2A''$
Vibrational normal mode				
a′ symmetry				
ν_1	3328 (3195)	3326 (3193)	3253 (3123)	3310 (3178)
ν_2	3210 (3082)	3190 (3062)	3126 (3001)	3208 (3080)
ν_3	1754 (1684)	1541 (1479)	1840 (1766)	3082 (2959)
ν_4	1391 (1335)	1429 (1372)	1371 (1316)	1394 (1338)
ν_5	1209 (1161)	1352 (1298)	1105 (1061)	1306 (1254)
ν_6	963 (924)	993 (953)	918 (881)	991 (951)
ν_7	704 (676)	777 (746)	492 (472)	542 (520)
ν_8	433 (416)	461 (443)	349 (335)	283 (272)
ν_9	370 (355)	365 (350)	229 (220)	185 (178)
a″ symmetry				
ν_{10}	901 (865)	958 (920)	913 (876)	929 (892)
ν_{11}	727 (698)	566 (543)	688 (660)	426 (409)
ν_{12}	530 (509)	366 (351)	456 (438)	419 (402)

Table 5. Vertical excitation energies (eV) of neutral states of 1,1-C_2H_2FCl obtained at three computation levels. All the results were obtained with the aug-cc-pVDZ basis sets. In parentheses are shown the results obtained with the cc-pVDZ basis set.

	Description[a]			
ΔE (eV)	SAC–CI			
6.34	$\pi \rightarrow 3s$			
6.53	$\pi \rightarrow [\sigma^* + 4d]$			
6.7	$\pi \rightarrow \pi^*$			
7.38	$\pi \rightarrow 3p$			
7.59	$\pi \rightarrow 3p$			
8.18	$\sigma \rightarrow 3p\sigma + [\sigma^* + (Cl)]$			
	TDDFT			
M06-2X(M06-2X/cc-pVDZ)			PBE0	
ΔE (eV)	Description		ΔE (eV)	Description
6.58	$\pi \rightarrow [\sigma^* + 4d]$, $\pi \rightarrow 3s$		6.52	$\pi \rightarrow [\sigma^* + 4d]$, $\pi \rightarrow 3s$
6.71 (6.96)	$\pi \rightarrow 3s$, $\pi \rightarrow [\sigma^* + 4d]$		6.70	$\pi \rightarrow 3s$, $\pi \rightarrow [\sigma^* + 4d]$
6.96 (7.61)	$\pi \rightarrow \pi^*$		6.87	$\pi \rightarrow \pi^*$
7.5	$\pi \rightarrow 3p$		7.46	$\pi \rightarrow 3p$
7.66	$\pi \rightarrow 3p$,$\pi \rightarrow [\sigma^* + 4d]$		7.68	$\pi \rightarrow 3p$
8.14 (8.43)	$\sigma \rightarrow \pi^*$		7.77	$\sigma \rightarrow \pi^*$
8.21	$\sigma \rightarrow [\sigma^* + 4d]$, $\sigma \rightarrow 3p$, $\sigma \rightarrow 4d$		8.35	$\pi \rightarrow 4d$
8.42	$\pi \rightarrow 4d$		8.37	$\sigma \rightarrow 3s$, $\sigma \rightarrow [\sigma^* + 4d]$
8.56	$\pi \rightarrow 3p\pi$		8.63	$\pi \rightarrow 3p\pi$
8.83	$\sigma \rightarrow 3s$, $\sigma \rightarrow [\sigma^* + 4d]$		8.74	$\sigma \rightarrow 3s$, $\sigma \rightarrow [\sigma^* + 4d]$
8.87	$\pi \rightarrow 4d$		8.94	
9.15	$\pi_i \rightarrow [\sigma^* + 4d]$, $\pi_i \rightarrow 4d$, $\pi_i \rightarrow 3p$, $\pi_i \rightarrow 3s$		8.97	$\pi_i \rightarrow \pi^*$
9.29	$\pi_i \rightarrow \pi^*$		9.14	$\pi_i \rightarrow [\sigma^* + 4d]$, $\pi_i \rightarrow 3s$
9.31	$\pi \rightarrow 4s$		9.30	$\pi \rightarrow 4s$

[a]The ground-state electronic configuration is represented as $(\pi_i{}^2\sigma^2\pi^2)$ staying for $[(2a'')^2(9a')^2(3a'')^2]$. The σ MO has a pronounced n(Cl) character. When two configurations are mentioned, the dominant one is reported first and the π_i notation designates the internal π orbital.

Table 6. Optimised geometries of the first two excited states at several calculation levels. The atomic numbering refers to the figure in Table 2. Internuclear distances are given in Å and angles in degrees. The adiabatic excitation energies (eV) are listed in parentheses.

First excited state (correlates with $\pi \rightarrow [\sigma^* + 4d]$)					
Level	C1–C2	C2–H3	C2–H4	C1–F5	C1–Cl6
UM06 (4.58)	1.4194	1.0919	1.0856	1.3149	2.2566
TDDFT/M06-2X (4.67)	1.3925	1.093	1.0858	1.3154	2.2824
TDDFT/PBE0 (4.65)	1.3978	1.093	1.087	1.3197	2.2643
	H3–C2–C1	H4–C2–C1	F5–C1–C2	Cl6–C1–C2	
UM06	120.958	117.65	112.459	106.751	
TDDFT/M06-2X	120.670	118.024	114.690	104.062	
TDDFT/PBE0	121.230	117.970	113.570	106.880	
Second excited state (correlates with $\pi \rightarrow 3s$)					
Level	C1–C2	C2–H3	C2–H4	C1–F5	C1–Cl6
TDDFT/M06-2X (6.37)	1.4003	1.0889	1.092	1.2893	1.6601
	H3–C2–C1	H4–C2–C1	F5–C1–C2	Cl6–C1–C2	
TDDFT/M06-2X	118.573	118.880	120.173	122.115	
$\pi \rightarrow \pi^*$ state					
Level	C1–C2	C2–H3	C2–H4	C1–F5	C1–Cl6
TDDFT/M06-2X (6.47)	1.4690	1.0864	1.0853	1.3194	1.6590
TDDFT/PBE0 (6.42)	1.4701	1.0884	1.0871	1.3232	1.6634
	H3–C2–C1	H4–C2–C1	F5–C1–C2	Cl6–C1–C2	
TDDFT/M06-2X	118.940	118.584	119.950	121.735	
TDDFT/PBE0	118.994	118.783	119.988	121.863	

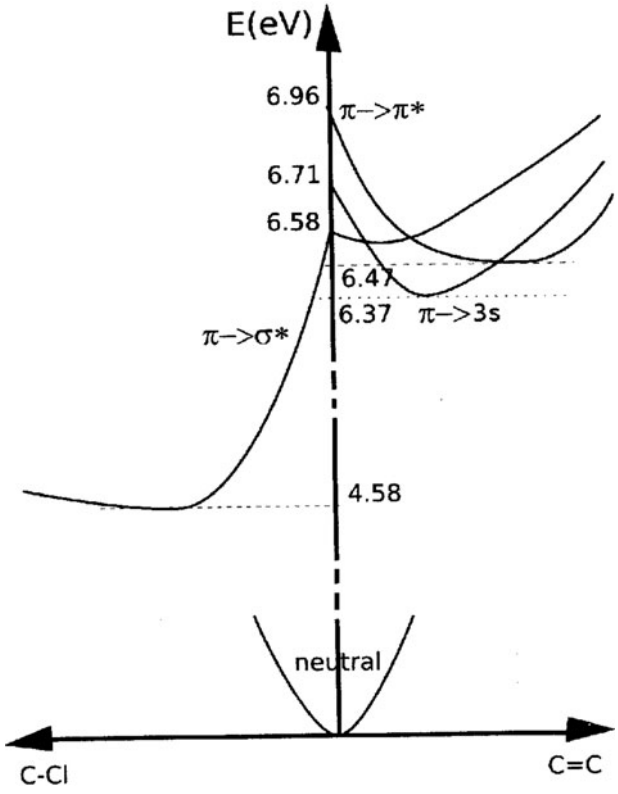

Figure 3. Schematic representation of the calculation results related to the first three excited states of 1,1-C_2H_2FCl.

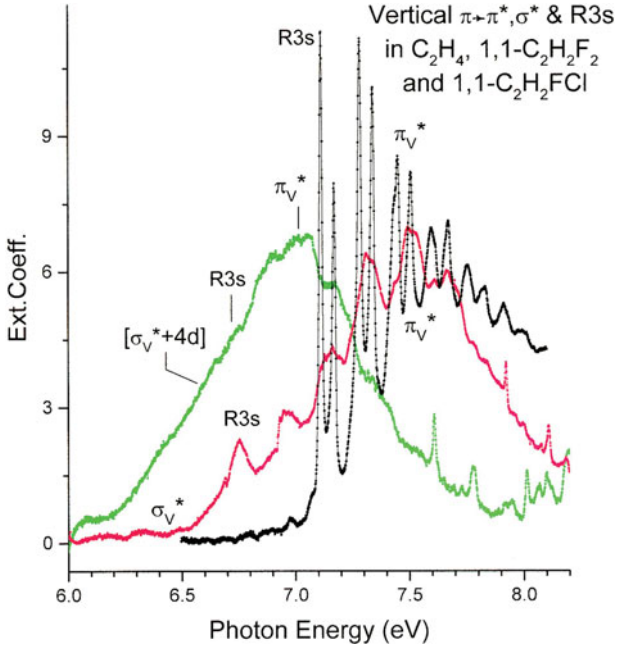

Figure 4. VUV photoabsorption spectra of C_2H_4 (black), 1,1-$C_2H_2F_2$ (red) and 1,1-C_2H_2FCl (green) on an expanded photon energy scale between 6.0 and 8.0 eV. The calculated vertical excitation energies to the valence (σ^*_v, σ^*_v + 4d and π^*_v) and the adiabatic excitation energy of the Rydberg (3s) orbitals are indicated for each molecule.

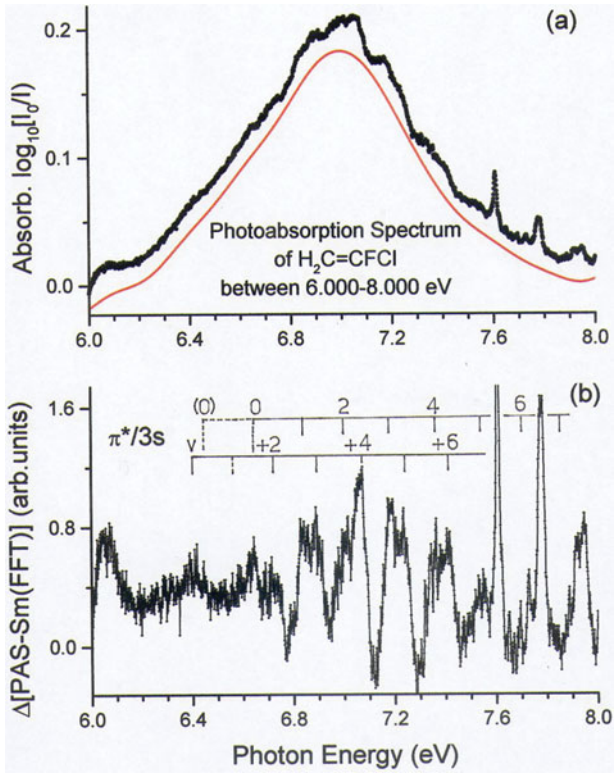

Figure 5. (a) VUV photoabsorption spectrum of 1,1-C_2H_2FCl on an expanded photon energy scale between 6.0 and 8.0 eV. The continuous (red) line is the FFT strongly smoothed spectrum. (b) **Δ** plot resulting from the subtraction of this continuum. Long vertical bars indicate the vibrationless (0,0) transitions of the valence and of the Rydberg transitions. For each transition, the progression is identified by short vertical bars and only the even quanta v are numbered.

5.1. The transitions in the 6.0–8.0 spectral region (see Figures 4 and 5)

The typical broadband of the ethylene derivatives has its maximum at 7.01 eV (56,540 cm^{-1}) in 1,1-C_2H_2FCl. Contrarily to the observations made in the PAS of C_2H_4 [1] and 1,1-$C_2H_2F_2$ [5], the vibrational structure essentially consists of broad and diffuse peaks. On the high energy side of the major band, several weak but sharp structures appear. The comparison of the same band in three different related compounds, i.e. C_2H_4 [1], 1,1-$C_2H_2F_2$ [5] and 1,1-C_2H_2FCl, as investigated in the present work, is very informative as shown in Figure 4, where the different contributions of valence and Rydberg transitions have been located.

Comparing these three compounds, the peak maximum observed in the PAS of 1,1-C_2H_2FCl obviously shows a significant red shift of about 0.5 eV. On the other hand, the position of this maximum does not change significantly when the H atoms are substituted by one [1] or two F atoms [5]. However, the substitution of an F atom by a Cl atom

Table 7. Positions in energy (eV), wave numbers (cm^{-1}) and assignments proposed for the features observed in the 7.01-eV band in the vacuum UV PAS of 1,1-C_2H_2FCl. Comparison is made with the observation and assignments of [6]. Conversion factor: 1 eV = 8065.545 cm^{-1} [16].

This work		[6]	Assignments	
(eV)	(cm^{-1})	(cm^{-1})	This work	[6]
6.398	51,603		3sR, $v = 0$	
(6.447)	51,999		($^1A''$, $v = 0$)[a]	
(6.592)	53,168		(3sR, $v = 1$)	
6.645	53,596		($^1A''$, $v = 0$)[a]	
6.719	54,192		3sR, $v = 2$	
6.839	55,160		$^1A''$, $v + 1$	
6.895	55,612		3sR, $v = 3$	
7.018	56,604	56,561	^{1}A″, $v + 2$	C–Cl stretch
7.073	57,048	57,100	3sR, $v = 4$	C═C stretch
7.192	58,007	57,887	$^1A''$, $v + 3$	C═Cl stretch
7.240	58,395	58,411	3sR, $v = 5$	C═C stretch
7.360	59,362	59,249	$^1A''$, $v + 4$	C═Cl stretch
7.416	59,814	59,773	3sR, $v = 6$	C═C stretch
7.530	60,733	60,606	$^1A''$, $v + 5$	
7.694	62,056		$^1A''$, $v + 6$	
7.869	63,468		$^1A''$, $v + 7$	

[a]For explanation and discussion, see text (Section 5.1).

seems to be crucial. This trend is confirmed by comparing the same spectral region in C_2H_3Cl [2] and C_2H_3Br [3], as performed in [5].

Owing to the weakness and the diffuseness of the structures in the 7.01-eV band displayed in Figure 5(a), the subtraction method described in Section 2.2 has been applied to disentangle its vibrational structure. The subtracted continuum (dotted (red) curve in Figure 5(a)) is obtained by FFT smoothing of the band. The resulting Δ plot is shown in Figure 5(b). It obviously shows a structure starting at about 6.4 eV and most of the features clearly exhibit a doublet structure. The proposed assignment to vibrational progressions is displayed in Figure 5(b). The intensity distribution of both progressions is bell shaped and is therefore related to the associated Franck–Condon factors, giving confidence in the proposed assignment.

As shown in Table 7, a first vibrational progression starts at 6.398 eV and extends at least up to $v + 6$ with an average $hc\omega = 175 \pm 6$ meV (1410 ± 50 cm^{-1}). A second vibrational progression starts at 6.645 eV with at least seven vibrational levels with an average wave number $\omega = 1410 \pm 80$ cm^{-1} (175 ± 10 meV), too. The assignment of these transitions to the $\pi(3a'')\rightarrow 3s(R)(^1A'')$ and the $\pi(3a'')\rightarrow\pi^*(4a'')(^1A')$ next electronic states is discussed below. For both states we assign the wave number of 1410 cm^{-1} to the ν_3(C═C stretching) vibration (see Figure 2 and Table 4). This is consistent with the excitation of one electron from the bonding $\pi(3a'')$ orbital. The comparison of Table 2 and 6 shows that the $\pi\rightarrow$3s and the $\pi\rightarrow\pi^*$ states are both characterised by a large increase of the C═C bond length.

The calculated adiabatic excitation energies (see Table 6) also show that the two states are expected to be very close in energy, in qualitative agreement with the experiment. The $\pi(3a'')\rightarrow\pi^*(4a'')$ state is slightly higher in energy than the $\pi(3a'')\rightarrow 3s$ (R) state. This ordering is identical for the calculated vertical excitation energies at the SAC-CI and TDDFT levels (see Table 5). We therefore assign the transitions with the experimental (adiabatic) excitation energy at 6.398 eV to $\pi(3a'')\rightarrow 3s(R)$ (which is perturbed by its interaction with $\pi(3a'')\rightarrow [\sigma^* + 4d]$). The calculated adiabatic energy is indeed very close, i.e. 6.37 eV (see Table 6). The transitions starting at an experimental adiabatic energy of 6.645 eV are then assigned to $\pi(3a'')\rightarrow\pi^*(4a'')$, for which the calculated adiabatic energy is in the 6.42–6.47 eV range.

The $\pi(3a'')\rightarrow 3s(R)$ electronic transition would then correspond to an effective quantum number $n^* = 1.95$ (quantum defect $\delta = 1.05$). This fairly low value of n^* results most probably from the large coupling between the $\pi(3a'')\rightarrow 3s(R)$ and the $\pi(3a'')\rightarrow[\sigma^* + 4d]$ configurations. Such Rydberg–valence interactions between 3s orbitals and antibonding σ^* valence orbitals lead frequently to a so-called rydbergisation along given dissociation pathways. This phenomenon has been observed in many different excited molecules with important consequences for their photochemical behaviour [31].

The other state resulting from this configuration interaction, which is denoted as '$\pi\rightarrow[\sigma^* + 4d]$, $\pi\rightarrow$3s' in Table 5 is calculated at lower energy (see Table 6 and Figures 3 and 4) and is most probably repulsive. It is therefore not surprising that no vibrational progression could be

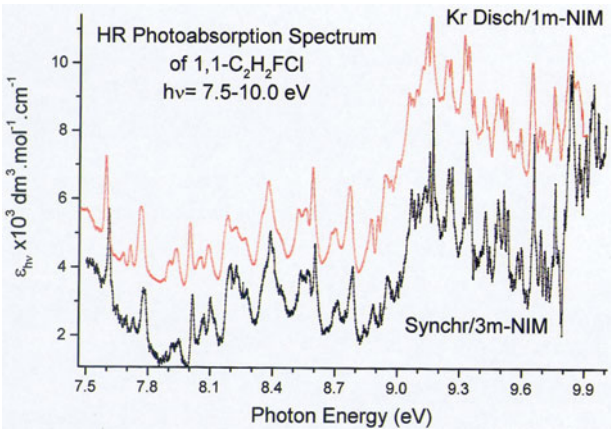

Figure 6. High-resolution VUV photoabsorption spectrum of 1,1-C_2H_2FCl between 7.5 and 10 eV photon energy obtained in the laboratory using the 1m-NIM monochromator and a discharge lamp (red line) and at BESSY using a 3m-NIM monochromator dispersing synchrotron radiation. The two spectra are slightly shifted on the *y*-scale for clarity.

observed in the corresponding energy range. At least a part of the subtracted continuum could be assigned to this state.

From this analysis based on the *ab initio* calculations, the $\pi(3a'')\rightarrow 3s$ Rydberg vertical transition energy is red shifted by about 0.4 eV with respect to C_2H_4 by halogen substitution (in $C_2H_2F_2$ and C_2H_2FCl) (see Figure 4). As shown in the figure, the $\pi(3a'')\rightarrow\pi^*(4a'')(^1A')$ vertical transition exhibits a small blue shift of about 0.1 eV in $C_2H_2F_2$ and a large red shift in C_2H_2FCl, i.e. of about 0.6 eV.

The wave number of 1410 cm^{-1} for ν_3 (see Figure 2) as determined in the present work can readily be compared with the value of 1350 cm^{-1} measured by Scott and Russell [6]. The major difference in the interpretation of the band at 7.01 eV between Scott and Russell [6] and the present work is that in the former the entire band is assigned to the $\pi\rightarrow\pi^*$ transition only. The vibrational structure is therefore accounted for by two vibrational wave numbers of about 1350 and 530 cm^{-1} assigned to C═C and C–Cl stretching vibrations, respectively [6]. However, considering the intensity distribution pattern of the vibrational structures as observed in Figure 5(b), progressions of two different electronic states are more probable.

5.2. *The transitions in the 7.8–10.4 eV spectral region (Figures 6 and 7)*

Part of this spectral region is shown in Figure 6 and exhibits an abundant structure superimposed on a weak continuum with a maximum measured at about 8.45 eV (68,154 cm^{-1}) in the present work (see Figure 1 and Table 1). This latter feature was assigned earlier to the $n(Cl)\rightarrow\sigma^*(C–Cl)$ valence transition [4]. Furthermore, a $n(Cl)\rightarrow\pi^*$ was expected at 9.27 eV [4]. The present calculations predict a quite more complex situation as it is shown in Table 5.

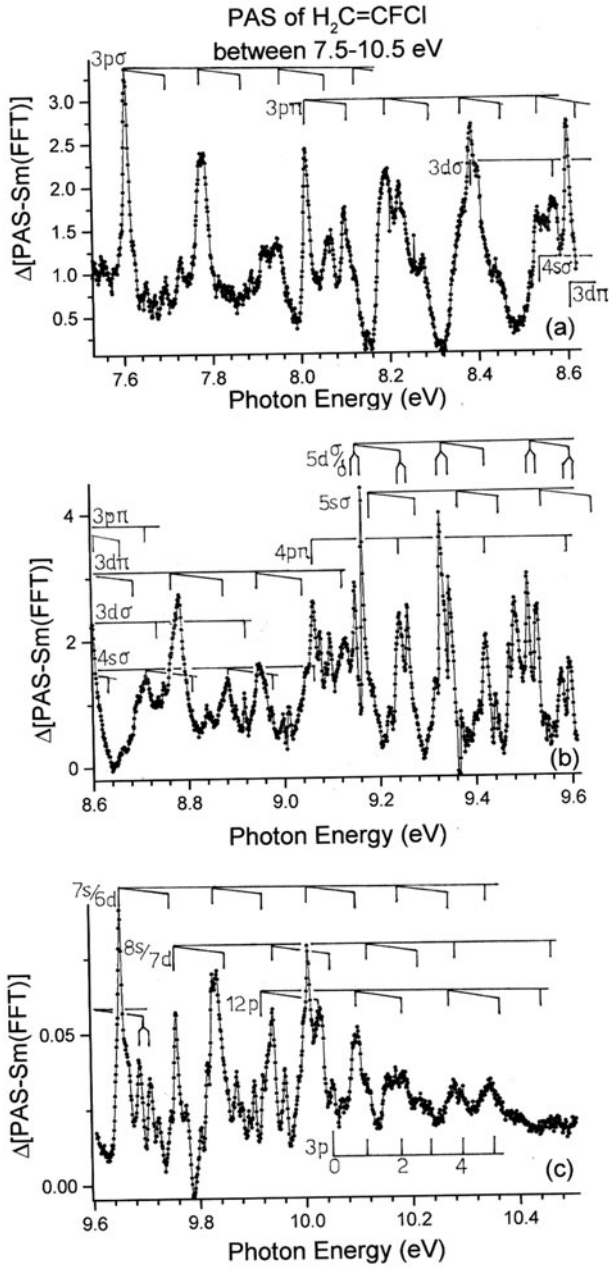

Figure 7. **Δ** plot of the VUV photoabsorption spectrum of 1,1-C_2H_2FCl on an expanded photon energy scale between 7.5 and 10.5 eV showing the details of the vibrational structure. The ν_9 vibrational component is not represented to avoid overcrowding.

At the TDDFT level, a $\sigma\rightarrow\pi^*$ transition (the σ MO has a *n*(Cl) character) is predicted around 8 eV, slightly below the $\sigma\rightarrow[\sigma^* + 4d]$ transition calculated at ~8.30 eV. According to the same calculations, several valence excited and Rydberg states lay close together and will very likely overlap in this region (see Table 5).

Figure 6 also shows the comparison between the PAS measured using the 1m-NIM at medium resolution and the 3m-NIM at higher resolution. This latter spectrum has been

handled by the subtraction procedure (see Section 2.2) and the result is shown in Figure 7(a)–(c).

All narrow and sharp features observed in this spectral region are assigned to transitions to Rydberg states which belong to series converging to ionisation energy limits associated with the different vibrational levels of a common electronic state, i.e. the $\tilde{X}^2A''$ ionic ground state. Figure 1 and Table 1 show the energy positions of the observed vibrationless Rydberg transitions.

To assign the observed spectral features, we assumed, as already mentioned, that the Rydberg formula is valid. Any significant perturbation due to Rydberg–Rydberg couplings is expected to induce repulsion of the zero-order energies and should be detected as poor quality fits to the Rydberg formula. In addition, in the absence of coupling between Rydberg series, the quantum defect has typical values which are characteristic of the angular momentum of the Rydberg orbital. When couplings are turned on, these values are perturbed. Such a situation already appeared in some of our previous investigations, where we could then highlight and quantitatively analyse transition between Hund's coupling cases [33]. The quantum defects are therefore important information. Consistent with our first zero-order hypothesis, we assume also that the vibrational structure within a transition to a given Rydberg state should be close to that of the cationic state to which the Rydberg series converges [34]. This argument involves constraints on both the energy and the intensity distribution. Here again, any discrepancy in the fits should be identified as a possible vibronic interaction. We emphasise that this procedure has been used successfully for the analysis of the VUV spectra of C_2H_3F [1] and 1,1-$C_2H_2F_2$[5].

The $3a''\rightarrow ns$ ($n \geq 4$) Rydberg transitions are observed up to $n = 8$ with an average quantum defect $\delta = 0.97 \pm 0.02$ compared to 0.90 observed previously [4]. This is a typical value for an *n*s series. In the present photon energy range, at least the transitions corresponding to $n = 4$ and $n = 5$ are characterised by vibrational progressions. The energy values listed in Table 1 correspond to adiabatic excitation energies.

The vertical bars in Figure 7 and the data listed in Table 8 show our assignments of the structures to vibrational progressions as obtained by the comparison of the $\tilde{X}^2A''$ HeI-PES to the Δ plot of the PAS. By this procedure, three vibrational normal modes are identified for the $3a''\rightarrow 4s$ transition and characterised by the wave numbers $\omega_A = 1420 \pm 50$ cm^{-1} (176 ± 6 meV), $\omega_B = 740 \pm 20$ cm^{-1} (92 ± 2 meV) and $\omega_C = 395 \pm 40$ cm^{-1} (49 ± 5 meV). In the HeI-PES of the $\tilde{X}^2A''$ ionic state [4], the wave numbers of 1400 ± 40 cm^{-1}, 720 ± 10 cm^{-1} and 380 ± 20 cm^{-1} were determined. By quantum chemical calculations (see Table 4), a′ vibrational normal modes (see Figure 2) are predicted for ν_3 at 1479 cm^{-1} (C═C stretching), ν_7 at 746 cm^{-1} (C–Cl stretching and H rocking) and ν_9 at 350 cm^{-1} (H rocking and C–F stretching). The good agreement between observed and predicted values gives us confidence in an assignment of the observed wave numbers $\omega_{A\ \text{to}}\ \nu_3$, $\omega_{B\ \text{to}}\ \nu_7$ and $\omega_{C\ \text{to}}\ \nu_9$ vibrational normal modes. In addition, the intensity ratios observed are similar to those of the photoelectron band.

The adiabatic excitation energy of the $3a''\rightarrow 5s$ Rydberg transition is observed at 9.186 eV. In this region, the spectrum becomes fairly to crowded. The short progression observed has been tentatively interpreted assuming the excitation of the same modes as for the $3a''\rightarrow 4s$ transition. Two wave numbers are identified at 1440 ± 20 cm^{-1} (179 ± 3 meV) and 660 ± 60 cm^{-1} (82 ± 8 meV). The first one corresponds very well to ω_3 whereas the second one is not incompatible with ω_7.

For the $3a''\rightarrow np$ Rydberg (n = 3–6 or 8) transitions, two different quantum defects are obtained and their average values are $\delta(np\sigma) = 0.63 \pm 0.04$ and $\delta(np\pi) = 0.40 \pm 0.04$. The dispersion of the quantum defect along the experimentally observable members of the series is fairly narrow. This should point towards the validity of the Rydberg formula and thus towards limited interstate couplings. To be rigorous on a symmetry basis (C_s point group), the $np\sigma$ and $np\pi$ orbitals should be denoted as npa' and npa'', respectively. However, if we assume that the molecular ion field is nearly cylindrical, i.e. diatomic like, it makes sense to use the σ, π, δ nomenclature. On this basis, the observed transitions are classified as shown in Table 1. In our earlier work [4] on the same system, δ values of 0.62 and 0.40 have been obtained. Similar observations have been reported in the study of the VUV spectrum of 1,1-$C_2H_2F_2$ [5]. In this latter case, the $3p\sigma$–$3p\pi$ energy splitting is 183 meV, whereas this quantity becomes 404 meV in the present molecular system. This observation is not unexpected. The $3p\sigma$–$3p\pi$ splitting results from the non-spherical nature of the molecular field, which is obviously more severe for the C_2H_2FCl molecule. Clearly, the $np\sigma$ transitions are observed up to $n = 6$, whereas the $np\pi$ transitions appear up to $n = 8$. As will be discussed later in this section, a transition observed at 9.920 eV could likely be assigned to the $12p\pi$ Rydberg state and characterised by $\delta = 0.451$.

Vibrational progressions could be identified for the $3p\sigma$, $3p\pi$ and $4p\pi$ Rydberg states. These are displayed in Figure 7 and the energies are listed in Table 8. For some spectral features, no clear unique assignment could be provided. In these cases, the energy values have been put in square brackets and possible tentative assignments have been suggested, but the interpretation is, in such cases, clearly much less reliable. The intensity of overlapping transitions is accounted for by considering the sum of the individual contributions. For the $3p\sigma$ and $3p\pi$ Rydberg states, well-defined progressions are observed and three different wave numbers can be inferred, i.e. $\omega_3 = 1450 \pm 20$ cm^{-1}

Table 8. Positions in energy (eV), corresponding wave numbers (cm^{-1}) and assignments proposed in the present work for the structures in the vacuum UV photoabsorption spectrum of 1,1-C_2H_2FCl in the 7.8–10.4 eV spectral region. In the fourth column, the average values of the energy and the wave numbers associated with the observed vibrational mode are indicated. Conversion factor: 1 eV = 8065.545 cm^{-1} [16].

Energy (eV)[a]	Wave number (cm^{-1})	Assignments	
	$3a'' \rightarrow 3p\sigma$		
7.608	61,363	0	$\omega_3 = 180 \pm 3$ meV
7.652	61,717	na	1450 ± 20 cm^{-1}
7.67	61,863	ν_9	$\omega_7 = 81 \pm 7$ meV
7.695	62,064	ν_7	650 ± 60 cm^{-1}
7.730	62,347	$3\nu_9$	$\omega_9 = 45 \pm 4$ meV
7.785	62,790	ν_3	360 ± 30 cm^{-1}
7.816	63,040	na	
7.837	63,210	$\nu_3 + \nu_9$	
7.873	63,500	$\nu_3 + \nu_7$	
7.888	63,621	na	
7.919	63,871	$\nu_3 + 3\nu_9$	
7.949	64,113	na	
7.967	64,258	$2\nu_3$	
[8.013]	64,629	$2\nu_3 + \nu_9$	
8.037	64,823	$2\nu_3 + \nu_7$	
[8.064]	65,040	na	
8.116	65,460	$2\nu_3 + 2\nu_9$	
[8.149]	65,726	$3\nu_3$	
	$3a'' \rightarrow 3p\pi$		
8.013	64,629	0	$\omega_3 = 172 \pm 4$ meV
[8.064]	65,040	ν_9	1390 ± 30 cm^{-1}
8.100	65,331	ν_7	$\omega_7 = 83 \pm 3$ meV
8.149	65,726	$3\nu_9$	670 ± 20 cm^{-1}
8.192	66,073	ν_3	$\omega_9 = 41 \pm 15$ meV
8.223	66,323	na	330 ± 120 cm^{-1}
8.235	66,420	$\nu_3 + \nu_9$	
8.275	66,742	$\nu_3 + \nu_7$	
8.314	67,057	$\nu_3 + 3\nu_9$	
8.362	67,444	$2\nu_3$	
8.422	67,928	$2\nu_3 + \nu_9$	
[8.446]	68,122	$2\nu_3 + \nu_7$	
8.475	68,355	na	
8.490	68,476	na	
[8.515]	68,678	$2\nu_3 + 3\nu_9$	
[8.533]	68,823	$3\nu_3$	
8.553	68,985	na	
[8.569]	69,114	$3\nu_3 + \nu_9$	
[8.601]	69,372	$3\nu_3 + \nu_7$	
8.630	69,606	$3\nu_3 + 3\nu_9$	
[8.664]	69,880	$3\nu_3 + 2\nu_7$	
8.704	70,202	$4\nu_3$	
8.737	68,985	na	
	$3a'' \rightarrow 3d\sigma$		
8.387	67,646	0	$\omega_3 = 177 \pm 5$ meV
8.437	68,049	ν_9	1430 ± 40 cm^{-1}
[8.515]	68,678	$3\nu_9$	$\omega_9 = 45 \pm 3$ meV
8.566	69,089	ν_3	360 ± 20 cm^{-1}
[8.601]	69,372	$\nu_3 + \nu_9$	
[8.663]	69,872	$\nu_3 + 2\nu_9$	
[8.703]	70,202	$\nu_3 + 3\nu_9$	
[8.737]	70,469	$2\nu_3$	
8.848	71,363	$2\nu_3 + 2\nu_9$	
8.893	71,646	$2\nu_3 + 3\nu_9$	
[8.918]	71,928	$3\nu_3$	

(*continued*)

Table 8. (*Continued*).

Energy (eV)[a]	Wave number (cm^{-1})	Assignments	
	$3a'' \rightarrow 4s\sigma$		
8.535	68,839	0	$\omega_3 = 176 \pm 6$ meV
8.630	69,606	ν_7	$1420 \pm 50\ cm^{-1}$
8.676	69,977	$3\nu_9$	$\omega_7 = 92 \pm 2$ meV
8.712	70,267	ν_3	$740 \pm 20\ cm^{-1}$
[8.764]	70,687	$\nu_3 + \nu_9$	$\omega_9 = 49 \pm 5$ meV
8.803	71,001	$\nu_3 + \nu_7$	$395 \pm 20\ cm^{-1}$
8.846	71,348	$\nu_3 + 3\nu_9$	
[8.882]	71,638	$2\nu_3$	
8.933	72,050	$2\nu_3 + \nu_9$	
8.974	72,380	$2\nu_3 + \nu_7$	
9.045	72,953	$2\nu_3 + 3\nu_9$	
9.064	73,106	$3\nu_3$	
	$3a'' \rightarrow 3d\pi$		
8.601	69,372	0	
8.690	70,090	ν_7	$\omega_3 = 176 \pm 3$ meV
8.777	70,791	ν_3	$1420 \pm 20\ cm^{-1}$
8.832	71,235	$\nu_3 + \nu_9$	$\omega_7 = 89 \pm 3$ meV
8.869	71,533	$\nu_3 + \nu_7$	$720 \pm 20 cm^{-1}$
[8.918]	71,928	$\nu_3 + 3\nu_9$	$\omega_9 = 50 \pm 8$ meV
8.950	72,187	$2\nu_3$	$400 \pm 60\ cm^{-1}$
9.010	72,670	$2\nu_3 + \nu_9$	
9.035	72,872	$2\nu_3 + \nu_7$	
9.129	73,630	$3\nu_3$	
	$3a'' \rightarrow 4p\pi$		
9.065	73,114	0	$\omega_3 = 173 \pm 7$ meV
9.127	73,614	ν_9	$1395 \pm 60\ cm^{-1}$
9.209	76,575	$3\nu_9$	$\omega_9 = 48 \pm 6$ meV
[9.244]	76,913	ν_3	$390 \pm 50\ cm^{-1}$
9.386	77,341	$\nu_3 + 3\nu_9$	
9.423	77,824	$2\nu_3$	
9.564	78,107	$2\nu_3 + 3\nu_9$	
9.594	78,550	$3\nu_3$	
9.757	78,905	$4\nu_3$	
	$3a'' \rightarrow 5s\sigma$		
9.186	74,090	0	$\omega_3 = 179 \pm 3$ meV
9.282	74,864	ν_7	$1440 \pm 20\ cm^{-1}$
9.369	75,586	ν_3	$\omega_7 = 82 \pm 8$ meV
9.448	76,203	$\nu_3 + \nu_7$	$660 \pm 60\ cm^{-1}$
9.544	76,978	$2\nu_3$	
9.621	77,599	$2\nu_3 + \nu_7$	
9.723	78,421	$3\nu_3$	
9.800	79,042	$4\nu_3$	
	$3a'' \rightarrow 4d\sigma$ (doublet)		
9.151	73,808	0	$\omega_3 = 180 \pm 2$ meV
9.166	73,929	0	$1450 \pm 20\ cm^{-1}$
9.209	74,276	ν_9	$\omega_7 = 93 \pm 1$ meV
9.222	74,380	ν_9	$750 \pm 8\ cm^{-1}$
9.244	74,558	$3\nu_9$	$\omega_9 = 59 \pm 8$ meV
9.260	74,687	$3\nu_9$	$480 \pm 60\ cm^{-1}$
9.329	75,243	ν_3	Splitting Δ
9.347	75,389	ν_3	$\Delta = 18 \pm 2$ meV
9.381	75,663	$\nu_3 + \nu_9$	$145 \pm 20\ cm^{-1}$
9.398	75,780	$\nu_3 + \nu_9$	
9.422	75,994	$\nu_3 + \nu_7$	
9.510	76,703	$2\nu_3$	

(*continued*)

Table 8. (*Continued*).

Energy (eV)[a]	Wave number (cm^{-1})	Assignments	
9.527	76,840	$2\nu_3$	
9.579	77,260	$2\nu_3 + \nu_7$	
[9.596]	77,397	$2\nu_3 + \nu_7$	
9.688	78,139	$3\nu_3$	
9.709	78,308	$3\nu_3$	
	$3a''\rightarrow 7s\sigma/6d$		
9.654	77,865	0	$\omega_3 = 173 \pm 7$ meV
9.708	78,300	ν_9	1395 ± 60 cm^{-1}
9.747	78,615	ν_7	$\omega_7 = 93 \pm 10$ meV
9.776	78,849	$3\nu_9$	750 ± 80 cm^{-1}
9.829	79,276	ν_3	$\omega_9 = 60 \pm 5$ meV
9.88	79,688	$\nu_3 + \nu_9$	480 ± 40 cm^{-1}
9.933	80,115	$\nu_3 + \nu_7$	
9.961	80,341	$\nu_3 + 3\nu_9$	
10.006	80,704	$2\nu_3$	
10.069	80,212	$2\nu_3 + \nu_9$	
10.089	81,373	$2\nu_3 + \nu_7$	
10.156	81,914	$2\nu_3 + 3\nu_9$	
10.184	82,140	$4\nu_3$	
10.347	83,454	$5\nu_2$	
	$3a''\rightarrow 8s\sigma/7d$		
9.758	78,704	0	$\omega_3 = 178 \pm 4$ meV
9.802	79,058	ν_9	1440 ± 30 cm^{-1}
9.851	79,454	ν_7	$\omega_7 = 91 \pm 3$ meV
9.893	79,792	na	730 ± 20 cm^{-1}
9.940	80,172	ν_3	$\omega_9 = 46 \pm 2$ meV
9.987	80,551	ν_9	370 ± 20 cm^{-1}
[10.030]	80,897	ν_7	
10.075	81,260	$3\nu_9$	
10.113	81,567	$2\nu_3$	
10.291	83,003	$3\nu_3$	
10.441	84,212	$4\nu_3$	
	$3a''\rightarrow 12p\pi$		
9.920	80,010	0	$\omega_3 = 175 \pm 7$ meV
[10.030]	80,889	ν_9	1410 ± 60 cm^{-1}
10.098	81,446	ν_3	$\omega_7 = 97 \pm 17$ meV
10.278	82,898	$2\nu_3$	780 ± 100 cm^{-1}
10.373	83,583	ν_9	$\omega_9 \approx 50$ meV
10.425	84,083	$3\nu_7$	400 cm^{-1}
10.445	84,246	$3\nu_3$	

[a]Energy positions assigned to two or more transitions are given in square brackets.

(180 ± 3 meV), $\omega_7 = 650 \pm 60$ cm^{-1} (81 ± 7 meV) and $\omega_9 = 360 \pm 30$ cm^{-1} (45 ± 4 meV) for the $3p\sigma$ Rydberg state; and $\omega_3 = 1390 \pm 30$ cm^{-1} (172 ± 4 meV), $\omega_7 = 670 \pm 20$ cm^{-1} (83 ± 3 meV) and $\omega_9 = 330 \pm 120$ cm^{-1} (41 ± 15 meV) for the $3p\pi$ Rydberg state. The present measurements agree, but with a higher accuracy, with the observations reported earlier [4], i.e. with a vibrational spacing ranging from 1380 to 1460 cm^{-1} and a low energy spacing of 320 cm^{-1} in the $3p\sigma$ Rydberg state. However, for ω_7, the agreement with the theoretical predictions (see Table 4) is not as satisfactory, so that this assignment can be questioned.

At the end of the energy range considered in this section, weak but fairly sharp and close features are observed up from 9.920 eV (see Figure 7(c) and Table 8). These structures could be assigned to vibrational progressions where $\omega_3 = 1410 \pm 56$ cm^{-1} (175 ± 7 meV), $\omega_7 = 780 \pm 80$ cm^{-1} (97 ± 10 meV) and $\omega_9 \approx 403$ cm^{-1} (50 meV). Assuming the adiabatic excitation to be at 9.920 eV, an effective quantum number $n^* = 11.549$ is obtained and the transition is therefore assigned to $3a''\rightarrow 12p\pi$.

Compared to our earlier investigation [4], owing to the better resolution achieved in the present work, many sharp and very narrow features (about 5 meV full width half

maximum [FWHM] at 9.7 eV) can be observed. Several 3a″→*n*d Rydberg transitions are observed. They have been classified on the basis of their respective quantum defects. As for the *n*p series, at least two from the three *n*d series are likely to be observed, i.e. an ndσ series with $\delta = 0.13 \pm 0.03$ and an *n*dπ series with $\delta = -0.11 \pm 0.02$. Both series are observed up to $n = 6$ or 7. However, for the higher *n* values, *n*d and *n*s states are very close in energy and are expected to interact more or less strongly. In our earlier work, only one quantum defect value of 0.12 could be obtained [4]. A similar situation has been observed in the VUV PAS of 1,1-$C_2H_2F_2$ [5], where the energy difference between 3dσ and 3dπ is 109 meV. This splitting becomes 390 meV in the present 1,1-C_2H_2FCl molecular system. The propensity of an increase of the σ–π splitting with the increase of the atomic number of the substituent was already observed for the *n*pσ- and *n*pπ-Rydberg series. However, simultaneously, the symmetry lowering of the molecular system resulting from the chemical substitution breaks the spherical symmetry and induces an increase of the energy spacing between states differing by the projection of their orbital angular momentum.

From 9.151 eV upwards, closely lying very narrow doublets are observed. The first doublet corresponds to 9.151 and 9.166 eV (see Table 8). Using an average adiabatic excitation energy of 9.158 eV and $IE_{ad} = 10.024$ eV, an effective quantum number $n^* = 3.963$ and a quantum defect $\delta = 0.047$ are obtained indicating that we are likely dealing with 3a″→4d Rydberg transition.

As a further proposal, these signals are classified into two different vibrational progressions likely corresponding to two 4d-Rydberg transitions separated by a constant splitting of 145 ± 20 cm^{-1} (18 ± 2 meV) and characterised by quantum defects $\delta = 0.052$ and $\delta = 0.018$, successively. Both components of this doublet exhibit a vibrational structure very clearly consisting of the wave numbers $\omega_3 = 1450 \pm 20$ cm^{-1} (180 ± 2 meV), $\omega_7 = 750 \pm 8$cm^{-1} (93 ± 1 meV) and $\omega_9 = 480 \pm 60$ cm^{-1} (59 ± 8 meV). This doublet could be assigned to 4dπ/4dδ Rydberg transitions characterised by small quantum defects. The core containing less π- and δ-type orbitals than σ orbitals is expected to interact less with π and δ Rydberg orbitals than with σ ones. They should therefore be characterised by smaller quantum defects.

Table 8 and Figure 7 show the proposed vibrational analysis pertaining to 7s/6d and 8s/7d Rydberg states. For these states, the vibrational structure consists of the three following wave numbers: $\omega_3 = 1390 \pm 60$ cm^{-1} (173 ± 7 meV) and 1440 ± 30 cm^{-1} (178 ± 4 meV), $\omega_7 = 750 \pm 80$cm^{-1} (93 ± 10 meV) and 730 ± 20 cm^{-1} (91 ± 3 meV) and $\omega_9 = 480 \pm 40$ cm^{-1} (60 ± 5 meV) and 370 ± 20 cm^{-1} (46 ± 2 meV). Once again, we find very consistently the presence of the same modes as for the other Rydberg series. However, here, the excitation of the ω_9 mode in the 7s/6d state is questionable.

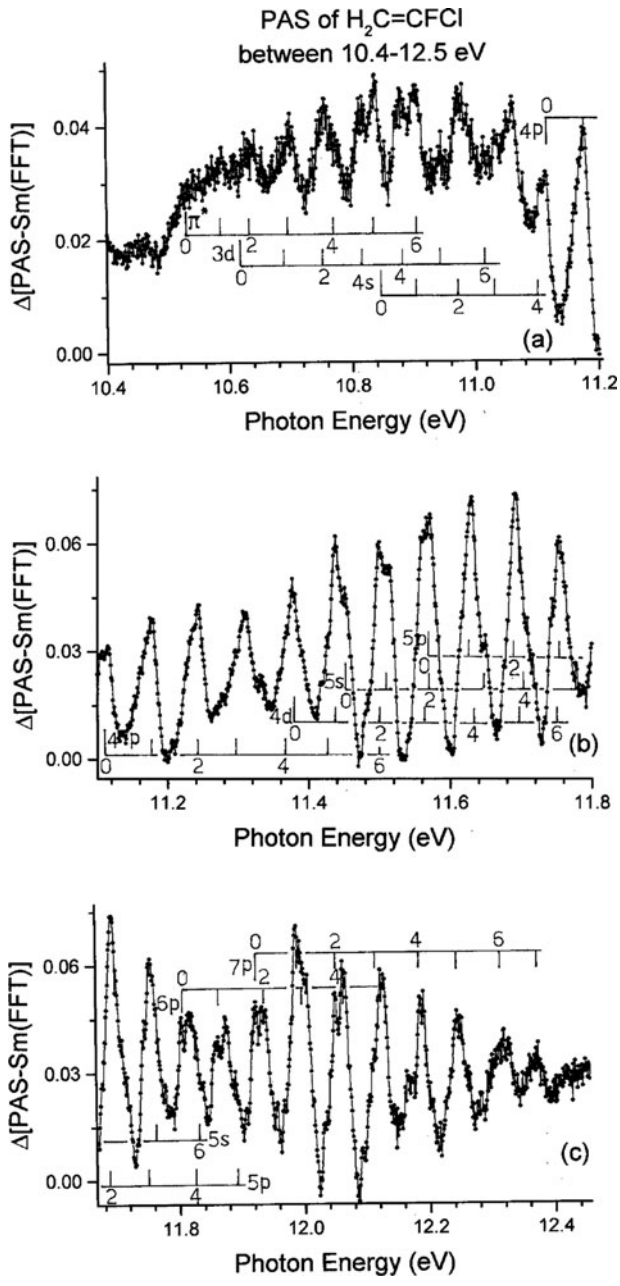

Figure 8. **Δ** plot of the VUV photoabsorption spectrum of 1,1-C_2H_2FCl on an expanded photon energy scale between 10.4 and 12.5 eV showing the details of the vibrational structure.

5.3. The transitions in the 10.4–12.5 eV spectral region (Figure 8)

As shown in Figure 1, this part of the spectrum exhibits two quite characteristic parts: (1) a broad and strong continuum underlying quite diffuse, very weak structures and (2) a very regular series of sharp but weak structures superimposed on a strong continuum.

Concerning the continua, their maximum can be measured on the FFT smoothed spectrum shown in Figure 1, i.e. at 10.93 eV (88,160 cm^{-1}) and at 11.70 eV (94,450 cm^{-1}),

successively. The absorption at 10.93 eV has been assigned to the $\sigma_{CH} \rightarrow \pi^*$ or $n_F \rightarrow \sigma^*$ transitions [4]. The continuum at 11.70 eV was assigned to an $n_F/\sigma_{CH} \rightarrow 3p$ Rydberg transition as predicted at 11.8 eV [4]. The narrow features between 11.4 and 12.4 eV have not been analysed in our earlier work. To allow us to perform a more detailed analysis of this spectral region the subtraction method has been applied (see section 2.2). The Δ plot provided by this procedure is shown in Figure 8(a)–(c).

The Rydberg series observed in this energy range has to converge to excited electronic states of the 1,1-$C_2H_2FCl^+$ cation. The first excited state $\tilde{A}^2A'$ (1,1-$C_2H_2FCl^+$) has been detected at 12.236 eV by HeI-PES [4]. This state is characterised by a long vibrational progression with a small wave number $\omega = 520 \pm 30\,cm^{-1}$. Very few Rydberg series converging to this ionisation limit are actually observed. Those observed in the present spectrum are listed in Table 1.

In our earlier work, only the $9a' \rightarrow ns$ transitions were mentioned [4]. In the present higher resolution work, the analysis also reveals additional series which could be assigned to transitions to *n*p and *n*d Rydberg states. Their vibrational analysis allowed us to observe mainly $9a' \rightarrow np$ type Rydberg transitions.

The lowest member of the $9a' \rightarrow ns$ Rydberg series is predicted to be close to 9.15 eV, i.e. at about the same energy as the $3a'' \rightarrow 4d\sigma$ transition (see Section 5.2). The vibrational analysis strongly suggests the latter assignment. Very likely the $9a' \rightarrow 3s$ Rydberg transition could be hidden in the 9.27-eV continuum. The two higher members of the *n*s series, exhibiting a vibrational progression, could be characterised by an average quantum defect $\delta = 0.87 \pm 0.03$. This value has to be compared with $\delta = 0.90$ as determined earlier [4].

A longer Rydberg series is observed up to $n = 7$ with an average quantum defect $\delta = 0.46 \pm 0.06$ which suggests a $9a' \rightarrow np$ assignment. Two additional members of a series are observed with their vibrational structure and correspond to an average quantum number of 0.06 ± 0.04. This suggests an assignment to an *n*d series.

Above 10.2 eV, the extinction coefficient sharply increases and peaks at about 10.8 eV (see Figure 1). In a term scheme based on experimental data, valence–valence excitation energies were predicted at 10.5 and 10.8 eV and assigned to $n_F \rightarrow \sigma^*_{C-Cl}$ and π^* transitions, respectively [4]. Superimposed on this strong feature, several very weak structures are observed. Above 11.0 eV the structure becomes stronger. In spite of their weakness and diffuseness, an analysis and assignments have been attempted.

The Δ plot in this energy range shows fairly clearly a vibrational structure for which several peaks seem to have a doublet structure. Using the HeI-PES data related to the $\tilde{A}^2A'$ band [4] as a reference, the 10.5–11.1 eV region could be decomposed into three vibrational progressions. The energy positions are listed in Table 9.

Starting at 10.534 eV, a vibrational progression of a single wave number is observed. A second progression with about the same vibrational spacing starts likely at 10.626 eV. Using these two excitation energies and 12.236 eV as convergence limit, effective quantum numbers $n^* = 2.83$ and 2.91 are obtained. The latter value being close to that expected for a $9a' \rightarrow 3d$ type Rydberg transition, the former excitation energy at 10.534 eV is then assigned to a valence transition. Based on a qualitative simulation using the PES data information, a weak $9a' \rightarrow 4s$ Rydberg transition is very likely involved at 10.838 eV. Owing to the crowding of the spectrum in this range only four vibrational spacing could be detected.

As mentioned in the fourth column of Table 9, the vibrational wave numbers deduced for the valence-to-valence transition and for the $9a' \rightarrow 3d$ and $9a' \rightarrow 4s$ Rydberg transitions are surprisingly quite similar, i.e. around 500 cm^{-1}. The wave numbers characterising the 12 vibrational normal modes of the $\tilde{A}^2A'$ state of the 1,1-$C_2H_2FCl^+$ have been predicted by quantum chemical calculations (see Table 4). A normal mode corresponding to the stretching vibration of C–Cl combined with the F–CC and Cl–CC bending motions (ν_7) has been calculated at 492 cm^{-1}, in good agreement with the values determined for the valence–valence and valence–Rydberg transitions. Furthermore, with respect to the neutral ground state, the predicted geometry of the $\tilde{A}^2A'$ state (see Table 2) shows a strong decrease of the C–F and a very strong increase of the C–Cl bond length. The F–CC and Cl–CC bond angles also undergo strong modifications. These results point to the likelihood of the above assignment. Unfortunately, no such information is available for the valence σ^* state.

The extensive structure observed from 11.1 to 12.4 eV has been analysed in detail by the same procedure as described above. The HeI-PES band of the $\tilde{A}^2A'$ cation state has been used as a reference. The result of the analysis is shown in Figure 8(b) and 8(c) and the energy positions are listed in Table 9.

The entire spectral region could be accounted for by a series of Rydberg transitions characterised by their effective quantum number n^* as listed in Table 9. The successive adiabatic excitation energies are identified as well as the vibrational progressions, each consisting of a unique wave number which is observed in all states at an average of $515 \pm 15\,cm^{-1}$ (64 ± 2 meV). It is assigned to the ν_7 normal mode (see Table 4).

All our analyses have been performed using zero-order formula and based on *ab initio* calculations, as discussed in the first part of Section 5. We were not able to identify couplings which would result in energy perturbations exceeding the experimental uncertainties. A higher resolution is probably required for this purpose.

In addition, in the present spectra, no unexplained doublet appears, so that there is no indication that spin–orbit coupling might play a role. This is not unexpected since,

Table 9. Energy positions (eV), corresponding wave numbers (cm^{-1}) and assignments proposed in the present work for the structures in the vacuum UV photoabsorption spectrum of 1,1-C_2H_2FCl in the 10.4–12.5 eV spectral region. In the fourth column, the averaged values of the energy and the wave numbers associated with the observed vibrational modes are indicated. Conversion factor: 1 eV = 8065.545 cm^{-1} [16].

Energy (eV)[a]	Wave number (cm^{-1})		Assignments
	Valence–valence transition		
10.534	84,962	0	$\omega_7 = 61 \pm 8$ meV
10.584	85,366	ν_7	490 ± 60 cm^{-1}
10.638	85,801	$2\nu_7$	
10.700	86,301	$3\nu_7$	
10.770	86,866	$4\nu_7$	
10.838	87,414	$5\nu_7$	
10.906	87,963	$6\nu_7$	
	9a′→3p ($n^* = 2.495$)		
10.050	81,059	0	$\omega_7 = 61 \pm 8$ meV
[10.113]	81,567	ν_7	490 ± 60 cm^{-1}
[10.184]	82,140	$2\nu_7$	
10.250	82,672	$3\nu_7$	
10.313	83,180	$4\nu_7$	
10.378	83,704	$5\nu_7$	
10.444	84,236	$6\nu_7$	
	9a′→4s ($n^* = 3.119$)		
10.838	87,414	0	$\omega_7 = 67 \pm 5$ meV
[10.905]	87,955	ν_7	540 ± 40 cm^{-1}
10.977	88,535	$2\nu_7$	
11.037	89,019	$3\nu_7$	
11.108	89,592	$4\nu_7$	
	9a′→3d ($n^* = 2.907$)		
10.626	85,704	0	$\omega_7 = 66 \pm 5$ meV
10.687	86,196	ν_7	530 ± 40 cm^{-1}
10.757	86,761	$2\nu_7$	
10.818	87,253	$3\nu_7$	
10.883	87,777	$4\nu_7$	
10.948	88,302	$5\nu_7$	
11.022	88,898	$6\nu_7$	
	9a′→4p ($n^* = 3.484$)		
11.115	89,649	0	$\omega_7 = 64 \pm 4$ meV
11.175	90,132	ν_7	520 ± 30 cm^{-1}
11.244	90,689	$2\nu_7$	
11.307	91,197	$3\nu_7$	
11.368	91,762	$4\nu_7$	
[11.438]	92,254	$5\nu_7$	
[11.500]	92,753	$6\nu_7$	
	9a′→4d ($n^* = 3.980$)		
11.377	91,762	0	$\omega_7 = 63 \pm 2$ meV
[11.438]	92,254	ν_7	510 ± 20 cm^{-1}
[11.500]	92,754	$2\nu_7$	
11.567	93,294	$3\nu_7$	
[11.631]	93,810	$4\nu_7$	
[11.692]	94,302	$5\nu_7$	
11.754	94,802	$6\nu_7$	
	9a′→5p ($n^* = 4.506$)		
11.563	93,262	0	$\omega_7 = 65 \pm 4$ meV
[11.631]	93,810	ν_7	520 ± 30 cm^{-1}
11.692]	94,302	$2\nu_7$	
11.755	94,810	$3\nu_7$	
11.827	95,391	$4\nu_7$	
11.889	95,891	$5\nu_7$	

(*continued*)

Table 9. (*Continued*).

Energy (eV)[a]	Wave number (cm^{-1})	Assignments	
	9a′→5s ($n^* = 4.155$)		
11.448	74,090	0	$\omega_7 = 65 \pm 8$ meV
11.511	74,864	ν_7	520 ± 60 cm^{-1}
11.572	75,586	$2\nu_7$	
11.650	75,203	$3\nu_7$	
11.709	76,978	$4\nu_7$	
11.767	77,599	$5\nu_7$	
11.839	78,421	$6\nu_7$	
	9a′→6p ($n^* = 5.599$)		
11.804	95,206	0	$\omega_7 = 64 \pm 6$ meV
11.862	95,673	ν_7	520 ± 50 cm^{-1}
11.923	96,165	$2\nu_7$	
11.995	96,746	$3\nu_7$	
12.064	97,303	$4\nu_7$	
12.125	97,795	$5\nu_7$	
	9a′→7p ($n^* = 6.593$)		
11.928	96,205	0	$\omega_7 = 63 \pm 5$ meV
11.988	96,690	ν_7	510 ± 40 cm^{-1}
12.049	97,182	$2\nu_7$	
12.12	97,754	$3\nu_7$	
12.185	98,279	$4\nu_7$	
12.244	98,755	$5\nu_7$	
12.313	99,311	$6\nu_7$	
12.371	99,779	$7\nu_7$	

[a]Energy positions assigned to two or more transitions are given in square brackets.

first of all, all detected Rydberg states presumably are singlet states. Despite the presence of a chlorine atom, the spin-conserving rule is expected to remain a strong propensity rule in electronic transitions. Therefore, singlet–triplet transitions, if any, are expected to be very weak. Second, as the C_2H_2FCl molecule and its cation belong to the C_s point group, the cation electronic states to which the Rydberg states converge are non-degenerate, and therefore, possess no electronic orbital angular momentum. The angular momentum associated with the rotational motion is expected to bring about only very small splitting of the spin states, in any case not detectable under our experimental resolution conditions.

6. Conclusions

The measurement of the VUV PAS of 1,1-C_2H_2FCl at higher resolution by using synchrotron radiation enabled us to re-examine in greater detail the data from 5 to 15 eV photon energy. Valence–valence [$\pi(3a'')\rightarrow\pi^*$] and valence–Rydberg [$(\pi)3a''\rightarrow 3s$] transitions are involved at the low-energy end of the spectrum, i.e. between 6 and 7.5 eV. Interactions with the σ^* valence orbital and with the 4d Rydberg orbital are also highlighted. Quantum chemical calculation results are used to help the interpretation of this complex region. An assignment is proposed for the vibrational structure of both states. A comparison is made with previous interpretations proposed for the same type of transitions observed in C_2H_4 [1] and 1,1-$C_2H_2F_2$ [5].

In the 7.8–10.5 eV photon energy range, the abundant fine structure has been assigned to vibronic Rydberg transitions, i.e. $3a''\rightarrow ns$ ($n = 3$–8), $np\sigma$ and $np\pi$ ($n = 3$–6 and 3–8) and the three $nd\sigma$, $nd\pi$ and $nd\delta$ ($n = 3$–7 and 3–6). All involved Rydberg states belong to series which converge to the ionic ground state at 10.024 eV [4]. The vibrational structures associated with these transitions have been analysed as based on the first band of the 1,1-$C_2H_2FCl^+$ HeI-PES results [4]. This procedure allowed us to assign the observed structure to three vibrational modes (and their harmonics and combination): ν_3 (C═C and C–F stretching), ν_7 (C–Cl stretching) and ν_9 (F–CC and Cl–CC bending).

In the 10.5–12.5 eV spectral range, the structures have been assigned to Rydberg series converging to the second cationic state 1,1-$C_2H_2FCl^+$ ($\tilde{A}^2A'$) at 12.236 eV [4]. The detailed analyses allowed us to assign most of the features to vibrational excitation of the ν_7 motion (C–Cl stretching combined with F–CC and Cl–CC bending) (Table 4).

Acknowledgements

R. Locht and B. Leyh gratefully acknowledge the European Community for its support through its TMR (Contract EU-HPRI-1999CT-00028) and I3 (Contract R II 3 CT-2004–506008). D. Dehareng's contribution was supported by the Belgian programme

on Interuniversity Attraction Poles of the Belgian Science Policy (IAP n°P6/19).

Funding

We are indebted to the University of Liège and the Fonds de la Recherche Fondamentale Collective (FRFC) for financial support.

References

[1] R. Locht, B. Leyh, D. Dehareng, H.-W. Jochims, and H. Baumgärtel, Chem. Phys. **362**, 97 (2009).
[2] R. Locht, B. Leyh, K. Hottmann, and H. Baumgärtel, Chem. Phys. **220**, 207 (1997); H. Keller-Rudek, G.K. Moortgat, MPI-Mainz-UV-VIS Spectral Atlas of Gaseous Molecules. www.atmosphere.mpg.de/spectral-atlas-mainz.
[3] A. Hoxha, R. Locht, B. Leyh, D. Dehareng, K. Hottmann, H.-W. Jochims, and H. Baumgärtel, Chem. Phys. **260**, 237 (2000).
[4] G. Tornow, R. Locht, R. Kaufel, H. Baumgärtel, and H.-W. Jochims, Chem. Phys. **146**, 115 (1990).
[5] R. Locht, H.-W. Jochims, and B. Leyh, Chem. Phys. **405**, 124 (2012).
[6] J.D. Scott and B.R. Russell, J.Am. Chem. Soc. **94**, 2634 (1972).
[7] R. Carbonneau, E. Bolduc, and P. Marmet, Can. J. Phys. **51**, 505 (1973).
[8] P. Marchand and P. Veillette, Can. J. Phys. **54**, 1309 (1976).
[9] P. Marmet, Rev. Sci. Instrum. **50**, 79 (1979).
[10] R.Z. Morawski, Rev. Sci. Instrum. **53**, 540 (1982).
[11] P.D. Marchand, Can. J. Phys. **51**, 814 (1973).
[12] R. Carbonneau and P. Marmet, Can. J. Phys. **51**, 2202 (1973); Phys. Rev. A **9**, 1898 (1974); and references therein.
[13] P. Marmet and H.K. Nasrallah, Can. J. Phys. **63**, 1015 (1985).
[14] R. Locht, B. Leyh, W. Denzer, G. Hagenow, and H. Baumgärtel, Chem. Phys. **155**, 407 (1991).
[15] R. Locht, B. Leyh, D. Dehareng, K. Hottmann, and H. Baumgärtel, J. Phys. B **43**, 015102 (2010).
[16] P.J. Mohr, B.N. Taylor, and D.B. Newell, Rev. Mod. Phys. **80**, 633 (2008).
[17] M.J. Frisch, G.W. Trucks, H.B. Schlegel, G.E. Scuseria, M.A. Robb, J.R. Cheeseman, G. Scalmani, V. Barone, B. Mennucci, G.A. Petersson, H. Nakatsuji, M. Caricato, X. Li, H.P. Hratchian, A.F. Izmaylov, J. Bloino, G. Zheng, J.L. Sonnenberg, M. Hada, M. Ehara, K. Toyota, R. Fukuda, J. Hasegawa, M. Ishida, T. Nakajima, Y. Honda, O. Kitao, H. Nakai, T. Vreven, J.A. Montgomery, Jr, J.E. Peralta, F. Ogliaro, M. Bearpark, J.J. Heyd, E. Brothers, K.N. Kudin, V.N. Staroverov, R. Kobayashi, J. Normand, K. Raghavachari, A. Rendell, J.C. Burant, S.S. Iyengar, J. Tomasi, M. Cossi, N. Rega, J.M. Millam, M. Klene, J.E. Knox, J.B. Cross, V. Bakken, C. Adamo, J. Jaramillo, R. Gomperts, R.E. Stratmann, O. Yazyev, A.J. Austin, R. Cammi, C. Pomelli, J.W. Ochterski, R.L. Martin, K. Morokuma, V.G. Zakrzewski, G.A. Voth, P. Salvador, J.J. Dannenberg, S. Dapprich, A.D. Daniels, O. Farkas, J.B. Foresman, J.V. Ortiz, J. Cioslowski, and D.J. Fox, *Gaussian 09, Revision A.02* (Gaussian Inc., Wallingford, CT, 2009).
[18] T.H. Dunning, Jr, J. Chem. Phys. **90**, 1007 (1989).
[19] J. Cizek, Adv. Chem. Phys. **14**, 35 (1969).
[20] G.E. Scuzeria and H.F. Schaefer, III, J. Chem. Phys. **90**, 3700 (1989).
[21] Y. Zhao and D.G. Truhlar, Theor. Chem. Acc. **120**, 215 (2008).
[22] M. Ernzerhof and G.E. Scuseria, Chem. Phys. **110**, 5029 (1999).
[23] H. Nakatsuji and K. Hirao, J. Chem. Phys. **68**, 2053 (1978).
[24] C. Adamo and V.J. Barone, Chem. Phys. **110**, 6158 (1999); I. Ciofini and C. Adamo, J. Phys. Chem. A **111**, 5549 (2007).
[25] C. Van Caillie and R.D. Amos, Chem. Phys. Lett. **317**, 159 (2000).
[26] G. Herzberg, *Molecular Spectra and Molecular Structure. Vol 2: Infrared and Raman Spectroscopy* (D. Van Nostrand Co Ltd, Princeton, NJ, 1949).
[27] G. Herzberg, *Molecular Spectra and Molecular structure. Vol 3: Electronic Spectra and Electronic Structure of Polyatomic Molecules* (D. Van Nostrand Co Ltd, Princeton, NJ, 1967).
[28] P. Torkington and H.W. Thompson, Trans. Faraday Soc. **41**, 236 (1945).
[29] D.E. Mann, N. Acquista, and E. Plyler, J. Chem. Phys. **23**, 2122 (1955).
[30] J.R. Nielsen and J.C. Albright, J. Chem. Phys. **26**, 1566 (1957).
[31] M.N.R. Ashfold, G.A. King, M. Murdock, M.G.D. Nix, T.A.A. Oliver and A.G. Sage, Phys. Chem. Chem. Phys. **12**, 1218 (2010).
[32] R. Locht, D. Dehareng, and Leyh B., unpublished work.
[33] R. Locht, B. Leyh, A. Hoxha, D. Dehareng, H.W. Jochims, and H. Baumgärtel, Chem. Phys. **257**, 283 (2000); R. Locht, B. Leyh, A. Hoxha, H.W. Jochims, and H. Bumgärtel, Chem. Phys. **272**, 259 (2001); R. Locht, B. Leyh, H.W. Jochims, and H. Baumgârtel, Chem. Phys. **317**, 73 (2005); Chem. Phys. **365**, 109 (2009).
[34] M.B. Robin, *Higher Excited States of Polyatomic Molecules*, Vol 1. (Academic Press, New York, 1974).
[35] K.K. Irikura, R.D. Johnson III, and R.N. Kacker, J. Phys. Chem. A **109**, 8430 (2005).